Characterizing Spatial Relationships of the Interannual Variability of CMIP6 Carbon Flux Data

Willa Tobin[1], Gretchen Keppel-Aleks[1]

[1]University of Michigan, Climate and Space Engineering, Ann Arbor, MI, USA

Introduction

The carbon cycle represents the exchange of carbon between carbon reservoirs in the atmosphere, biosphere, and hydrosphere. The exchange between the ocean, atmosphere, and terrestrial biosphere is considered the short-term, or "fast", carbon cycle and occurs on time scales of 100 years or less. The long-term, or "slow", carbon cycle consists of carbon exchange from geological reservoirs and takes place over thousands of years (Bruhwiler et al., 2018). While a majority of carbon is held in the long-term geological reservoirs, we are interested in the variability in the short-term carbon cycle because it can impact the climate within our lifetime.

In 2020, 31.6 Pg of CO_2 was released into the atmosphere due to anthropogenic sources (Ritchie, 2020). About 50% of this is taken up by natural carbon sinks ("Ocean-Atmosphere CO2 Exchange", 2015), and as a result, atmospheric CO_2 levels increase by 2.6 ppm from 2019 to 2020 (Lindsey, 2020). NOAA reported 2020 as the second warmest year on record, with a temperature anomaly of 1 ^oC above the 20th-century average (Dahlman, 2021). We know that greenhouse gases lead to warming surface temperatures (add reference), but recent studies have also shown that temperature anomalies are impacting the net carbon flux (Wang et al., 2012). Understanding the mechanism controlling the net carbon flux into the land is becoming increasingly important as our environment is forced to adapt to growing levels of carbon dioxide in the atmosphere.

The primary mechanisms for carbon exchange between the land and atmosphere are photosynthesis (uptake of carbon by plants) and respiration (carbon release into the atmosphere). Photosynthesis at the ecosystem scale is called gross primary production (GPP) which is denoted as a mass flux rate (typically in units of grams of carbon per meter squared per year) of carbon into the land. Once atmospheric CO_2 is biologically fixed, it can be respired by plants (autotrophic or AR) or dead organic matter can be decomposed by bacteria and fungi in the soil (heterotrophic or HR). Similar to GPP, AR and HR are also denoted as mass flux rates of carbon into the atmosphere. The net carbon flow into the land is defined as net biospheric productivity (NBP) (Chapin et al., 2011).

Terrestrial carbon cycle fluxes show large variations on seasonal timescales and regional spatial scales. In tropical regions, plants can photosynthesize year-round, while in higher latitudes plants are dormant in the winter. Figure 1B shows the seasonality of temperature for each region. The temperate (green) and polar (blue) have temperature ranges of 25 ^oC and 20 ^oC respectively and dip below 0 ^oC during the winter

months whereas the tropical (red) average monthly temperature range is 8 K and never dips below freezing. These seasonal patterns are mirrored in the average monthly NBP for each zonal region (Figure 1C). In panel C, we can see the summer peak for the polar (blue line, ~6 Pg C $year^{-1}$) and temperate region (green line, ~24 Pg C $year^{-1}$), whereas the tropical region does not exhibit a strong seasonal cycle. Previous studies have illustrated the dependence of the tropical carbon cycle on the interannual variability of temperature due to the response of carbon fluxes to temperature anomalies (Wang et al., 2013). Here, we will expand this analysis to polar and temperate regions to characterize how temperature and carbon fluxes are coupled.

Other climate patterns, such as the El Nino Southern Oscillation, affect carbon exchange on an interannual scale by causing alternating warm and cool periods in the pacific regions. Figure 1A shows NBP data from CESM2 for a polar, temperate, and tropical region with the long term (20 year) and seasonal trends removed to highlight the interannual variability (IAV) of NBP for each region. Understanding the controls on these interannual variations will enhance our ability to predict future climate projections. If we know the mechanisms that control carbon uptake and the environmental sensitivities thereof, we will be able to predict how the earth will respond to different emission scenarios and adapt accordingly.

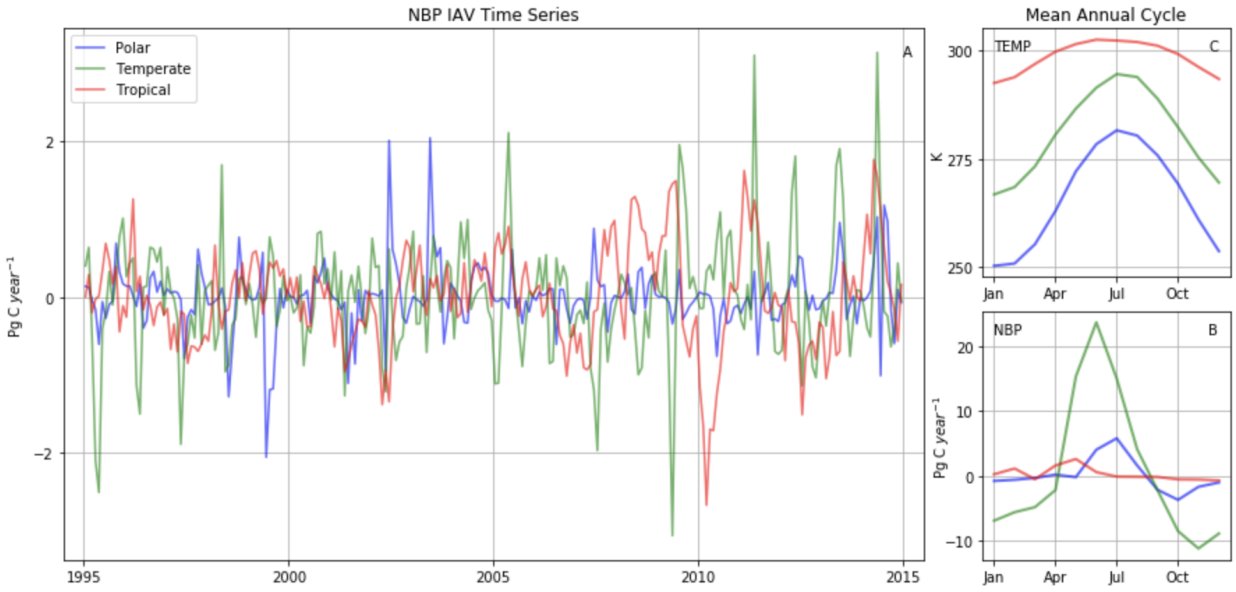

Figure 1. The main panel shows the detrended and deseasonalized zonaly aggregated NBP data. The two panels on the right show the mean annual cycle of the unprocessed zonaly aggregated NBP (flux of carbon into the land) and temperature data.

In this study, we will be exploring the relationships between the IAV of GPP, NBP, HR, and temperature. We perform correlation analysis on the most recent 20 years of historical (1995 to 2015) surface temperature and carbon flux data from CMIP6 earth system models (ESM) to quantify the relationships between each spatially aggregated variable.

Methods

The data used in our study comes from five ESMs from the Coupled Model Intercomparison Project Phase 6 (CMIP6). CMIP6 defines earth system models as global climate models that account for CO_2 fluxes between the biosphere, ocean, and atmosphere (Eyring et al., 2016). The five models we used are the Community Earth System Model version 2 (CESM2), Canadian Earth System Model version 5 (CanESM5), IPSL-CM6A-LR (IPSL), Norwegian Earth System Model version 2 (NorESM2), and MPI-ESM-1-1-HAM (MPI). We are using a set of 5 models to account for any uncertainty in model simulations.

For each model, we analyzed the last twenty years of the historical simulation (1995 to 2015) to focus on characterizing recent trends. Historical ESM simulations are based on forcing datasets that come from observations. Historical simulation forcings can vary between models, but generally include emissions of short-lived species and long-lived greenhouse gases, GHG concentrations, global gridded land-use forcing data sets, solar forcing, stratospheric aerosol data set (volcanoes), sea surface temperatures, and sea ice concentrations (Eyring et al., 2016).

The primary model used for our analysis is CESM2. Each CMIP6 model has slightly different parameterizations of earth system processes but typically uses the same historical forcing data sets. CESM2 uses CMIP6 provided forcings for the historical simulation combined with chemical and aerosol atmospheric constituents from anthropogenic and biomass burning it calculates itself. Other areas where CESM2 does not use CMIP6 forcings are for tropospheric oxidants for chemistry, stratospheric ozone for radiative effects, stratospheric aerosols for radiative effects, H_2O production rates due to CH_4 oxidation in the stratosphere, and N deposition to the land and ocean components (Danabasoglu et al., 2020).

We created three zonal regions to characterize tropical, temperate, and polar ecosystems with latitude bounds ranging from 0 ºN - 30 ºN, 30 ºN - 60 ºN, and 60 ºN - 90 ºN respectively. The carbon flux data from the model is given in units of [kg C m^{-2} s^{-1}]. To calculate the total zonal carbon flux for each time step, we summed the product of the flux at each grid cell with the corresponding area of each grid cell. The area of each grid cell was calculated using Equation 1, where R_{Earth} is the radius of the Earth, φ is longitude, and λ is latitude. The units were then converted from [kg C s^{-1}] to [Pg C $year^{-1}$]. Temperature data was aggregated by taking the zonal mean for each time step.

$$dA = (R_{Earth} * cos(\varphi)) * (R_{Earth} * \Delta\varphi * \Delta\lambda) \quad (1)$$

The long-term and seasonal trends of the zonally aggregated data were then removed to calculate the IAV of each data set. The long-term trend was removed by fitting a second-order polynomial to each zonally aggregated variable (from 1995 to 2015) and subtracting the second-order fitting. The seasonal cycles (e.g. Figures 1B and C) were removed by subtracting the monthly averages of the detrended data. We used this zonally aggregated, detrended, and deseasonalized data for the rest of our analysis.

After detrending and deseasonalizing the data, we found that the IAV in the carbon flux data for the winter months of the polar and temperate regions clustered around zero. This is a result of the models

parameterizing carbon fluxes to be zero after a seasonal/temperature threshold. To account for this, we removed the non-growing season months from our analysis by filtering out months where the zonal mean temperature is less than 0 ^{o}C. This led to October through April being removed from the high latitude zone, and the months of December through March being removed from the temperate zone.

We tested the coupling of each variable by calculating the Pearson correlation coefficient, r, of the monthly growing season IAV data. We used the python stats package linregress() function to generate r, p, and slope values. In addition to the monthly correlation, we calculated the direct correlation between the annual anomalies of the IAV data and the lagged correlation. The annual anomalies were calculated by subtracting the 1995 to 2015 mean of a given variable from the 1995 to 2015 annual means. The 20 year mean and annual means only include data from the growing season months. The lagged correlation was calculated by holding back the annual anomalies of one variable (generally the driver variable) by one year (i.e. correlation of 1995 - 2014 temperature data and 1996 - 2015 GPP data).

Results

The correlation and slope of temperature and each carbon flux differ across the three latitude zones we analyze. To account for the different seasonal cycles of each region we only considered months in the growing season as defined in the methods (months with a zonal mean temperature greater than 0 ^{o}C).

The polar region is temperature limited, as ecosystems are dormant in the winter so carbon exchange is restricted to the summer months. For every 1 ^{o}C increase in temperature, NBP increases by 0.37 Pg C year^{-1} (r = 0.37, Figure 2A), GPP increases by 0.84 Pg C year^{-1} (r = 0.40, Figure 2B), HR increases by 0.13 Pg C year^{-1} (r = 0.38, Figure 2C), and AR increases by 0.33 Pg C year^{-1} (r = 0.32, Figure 2D). The positive couplings of each flux with temperature show that even when only considering the growing season months with long-term and seasonal trends removed, temperature still exhibits controls over carbon exchange. For the polar region, GPP increases approximately twice (1.83x) as much for each 1 ^{o}C increase compared to total respiration (HR + AR), resulting in net uptake of CO_2 and the increased NBP cited above. Because fluctuations in respiration respond to fluctuations in carbon availability via GPP, respiration processes are also significantly correlated with GPP. For every 1 Pg C year^{-1} increase, HR increases by 0.09 Pg C year^{-1} (r = 0.53, Figure 2E) and AR increases by 0.47 Pg C year^{-1} (r = 0.96, Figure 2F).

The net carbon flux of the temperate region is less dependent on temperature than the polar region. For every 1 ^{o}C increase in temperature, NBP decreases by 0.15 Pg C year^{-1} (r = -0.09, Figure 2G), GPP increases by 0.96 Pg C year^{-1} (r = 0.29, Figure 2H), HR increases by 0.60 Pg C year^{-1} (r = 0.55, Figure 2I), and AR increases by 0.48 Pg C year^{-1} (r = 0.27, Figure 2J). The sign of the correlation between temperature and the component carbon fluxes (GPP/HR/AR) is the same as in the polar region, but the NBP temperature correlation becomes negative. This is due to the impact (slope) of temperature on HR increasing more than on GPP when compared to the polar region. The increase in respiration for the temperate region is now larger than the increase in GPP for every 1 ^{o}C increase by 0.12 Pg C year^{-1}. The correlation of respiration fluxes with GPP is similar in the temperate region compared to the polar region. For every 1 Pg C year^{-1} increase in GPP, HR increases by 0.13 Pg C year^{-1} (r = 0.39, Figure 2K) and AR increases by 0.49 Pg C year^{-1} (r = 0.92, Figure 2L).

There is a dramatic change in the impact of temperature on each carbon flux for the tropical region compared to the polar and temperate regions. For every 1 ^{o}C increase in temperature, NBP decreases by 0.66 Pg C year^{-1} (r = -0.42, Figure 2M), GPP decreases by 1.62 Pg C year^{-1} (r = -0.48, Figure 2N), HR decreases by 0.32 Pg C year^{-1} (r = -0.26, Figure 2O), and AR decreases by 0.62 Pg C year^{-1} (r = -0.34, Figure 2P). Increasing temperature now decreases the magnitude of each carbon flux. We speculate that this is because the mean temperature of the tropical region is close to the optimum temperature for photosynthesis, so increasing temperature will decrease plant productivity. Additionally, if higher temperatures are reducing GPP, there is less carbon to be respired thereby reducing respiration. Similar to the polar region, GPP decreases approximately double (1.72x) that of total respiration (HR + AR) for every 1 ^{o}C increase in temperature in the tropical region. The last two panels of Figure 2 (2Q and 2R) show that for every 1 Pg C year^{-1} increase in GPP, HR increases by 0.25 Pg C year^{-1} (r = 0.69), and AR increases by 0.47 Pg C year^{-1} (r = 0.86) respectively.

The relationships between production (GPP) and respiration (HR/AR) are independent of latitude. Figure 2 shows a strong positive correlation for each region between GPP and HR and AR. Focusing on GPP and AR, we found that the slope barely changes for each region (0.47 - 0.49 Pg C year^{-1} / Pg C year^{-1}). There is slightly more variability with latitude for GPP and HR (0.09 - 0.25 Pg C year^{-1} / Pg C year^{-1}) with the slope increasing from polar to tropical region. From the right two columns of Figure 2, we can infer that the relationship between ecosystems productivity and respiration is approximately constant across the regions we analyze.

The slopes for each region in Figure 2 show that the temperature sensitivity of NBP can be well approximated by the temperature sensitivity of the component fluxes in the balanced carbon budget. Specifically, we sum the temperature GPP, HR, and AR slopes (negative of HR and AR slopes) and compare them to the temperature NBP slope as seen in equation 2, where the subscript [T, m] denotes the slope of the correlation of that flux with temperature. The right side of equation 2 for the polar, temperate, and tropical regions are 0.38, -0.12, and -0.68 Pg C year^{-1} respectively. Comparing these numbers to the NBP temperature slopes for each region (0.37, -0.15, and -0.66 respectively), we can see that the balance is off by less than 0.03 Pg C year^{-1} for each region.

$$NBP_{T,m} \simeq GPP_{T,m} - HR_{T,m} - AR_{T,m} \quad (2)$$

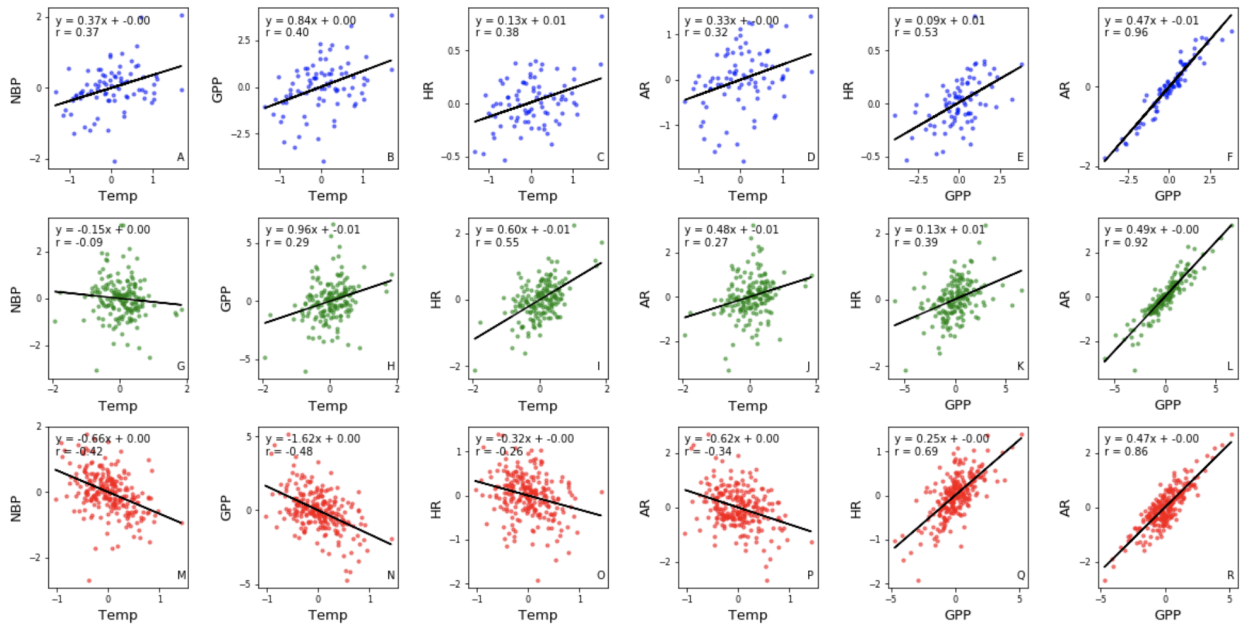

Figure 2. Scatter plots of detrended and deseasonalized zonaly aggregate growing season data. The First row uses data from the polar region, the second row uses data from the temperate region, and the third row uses data from the tropical region.

As expected, the direct IAV anomaly correlations calculated from annual data (Figure 3) show similar overall patterns to the monthly IAV correlations (Figure 2) for the temperate and tropical regions. The polar region correlation for temperature and AR/HR is significantly positive in Figure 1, whereas temperature and RT is showing a slightly negative correlation of the IAV anomalies. This difference could be due to the smaller number of growing season months in the polar region going into the annual anomaly making the correlation practically zero.

Our results show that after holding back one variable's anomalies by one year, most pairings have an insignificant correlation. The exceptions to this are for GPP and RT in the polar and temperate regions. For this test, we are assuming that the variable listed first in the x-axis of Figure 3 is the driving variable. For the polar and temperate regions, the annual anomaly of the IAV of GPP is showing a positive coupling to respiration in the following year ($r = 0.63$ and $r = 0.47$ respectively, Figure 3). The other significant lagged pairing is in the temperate region for temperature and lagged NBP. A positive anomaly of temperature IAV decreases the NBP IAV anomaly ($r = -0.41$, Figure 3). We can decompose this correlation by looking at the temperature and GPP x RT relationships. The direct correlation between temperature and GPP is positive, but not significant. Looking back at Figure 2H, we can see a significant positive correlation between temperature and GPP. We can then tie that to the significant positive lagged correlation of GPP and RT ($r = 0.47$, Figure 3). Assuming a positive temperature anomaly increases GPP for the temperate region, RT of the following year will be enhanced, thereby decreasing NBP of the following year.

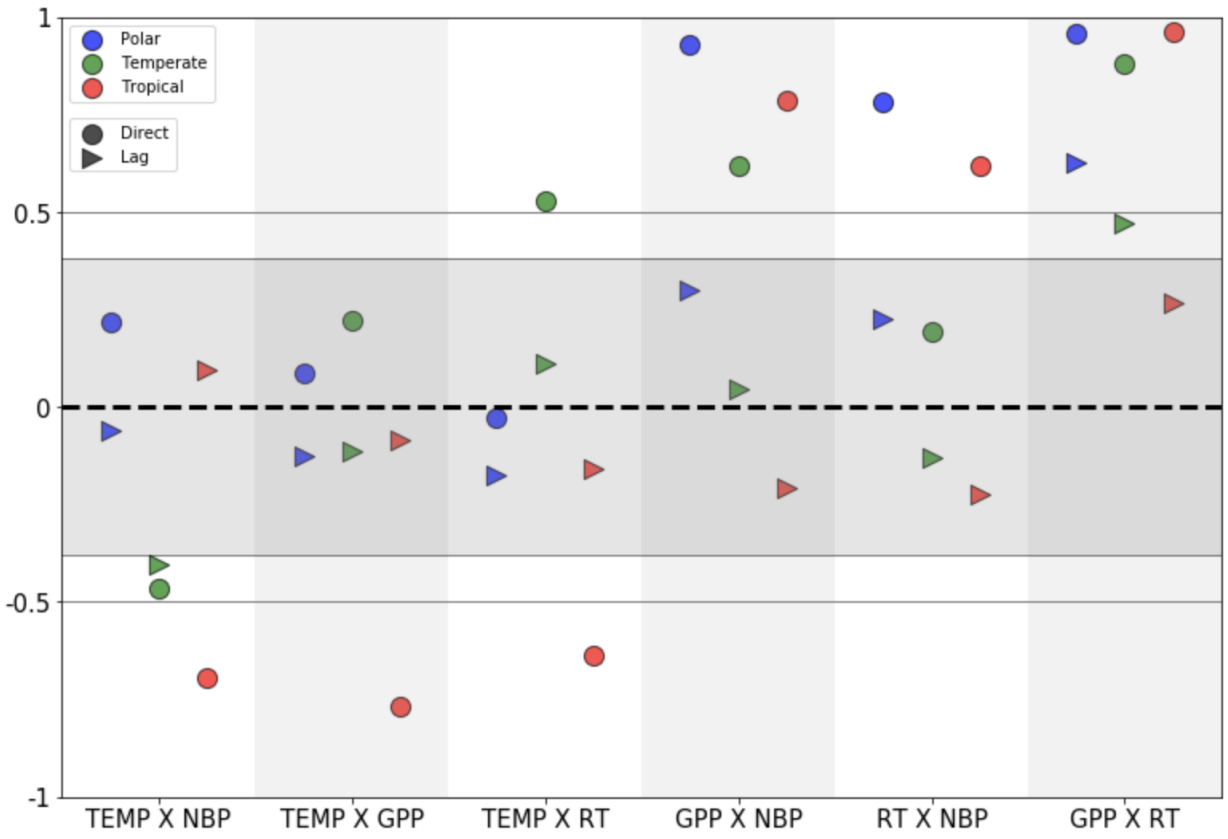

Figure 3. Scatter plot of correlations for direct and lagged data pairings. The data is the annual anomaly from 1995 - 2015 of detrended and deseasonalized growing season data. The horizontally shaded region represents insignificant correlation values.

The models show the most agreement in correlation strength in the temperate region (max spread of 0.30), and the least agreement in the tropical region (max spread of 1.07). Focusing on the first three columns of Figure 4, the models show modest positive correlations for TEMP x GPP and TEMP x RT for the polar and temperate regions. For the temperate region, these relationships result in a net-zero correlation for TEMP x NBP, indicating a similar magnitude slope of the linear TEMP x GPP and TEMP x RT fits, as seen in Figure 2G. The models show a larger spread in the polar region correlation magnitudes for TEMP x GPP and TEMP x RT which results in a similar spread in magnitude for TEMP x NBP. For the polar region, the TEMP x NBP correlations do not spread around zero. The polar region temperature correlations for each model have similar magnitudes, indicating that for each model, the slope of the linear TEMP x GPP fit is approximately double the slope of the linear TEMP x RT fit. This is consistent with the results from Figures 2A, 2B, and 2C.

Within our five model ensemble, we observed trends of specific models across regions and correlation pairs. The tropical respiration data from CanESM5 is consistently different from the other models, with the TEMP x RT and NBP x RT correlations having an opposite sign than the other models. MPI and NorESM2 have higher temperature sensitivity than the other models for the polar and tropical regions (respectively) as we can see the blue flags setting the upper end of the range and the red circles setting the

lower end of the range for the first three columns. On the other hand, IPSL has a low temperature sensitivity for the polar region due to all the temperature correlations sitting just above zero.

For each temperature variable pairing, there is a generally decreasing correlation strength from the polar to tropical region. For each carbon flux GPP pairing, the correlation strength is consistent across the regions. The correlation of NBP x RT is consistent for the temperate and tropical regions but stronger for the polar region. This brings back up the point of latitudinal sensitivity of IAV of carbon fluxes to temperature vs insensitivity of carbon flux couplings to latitude.

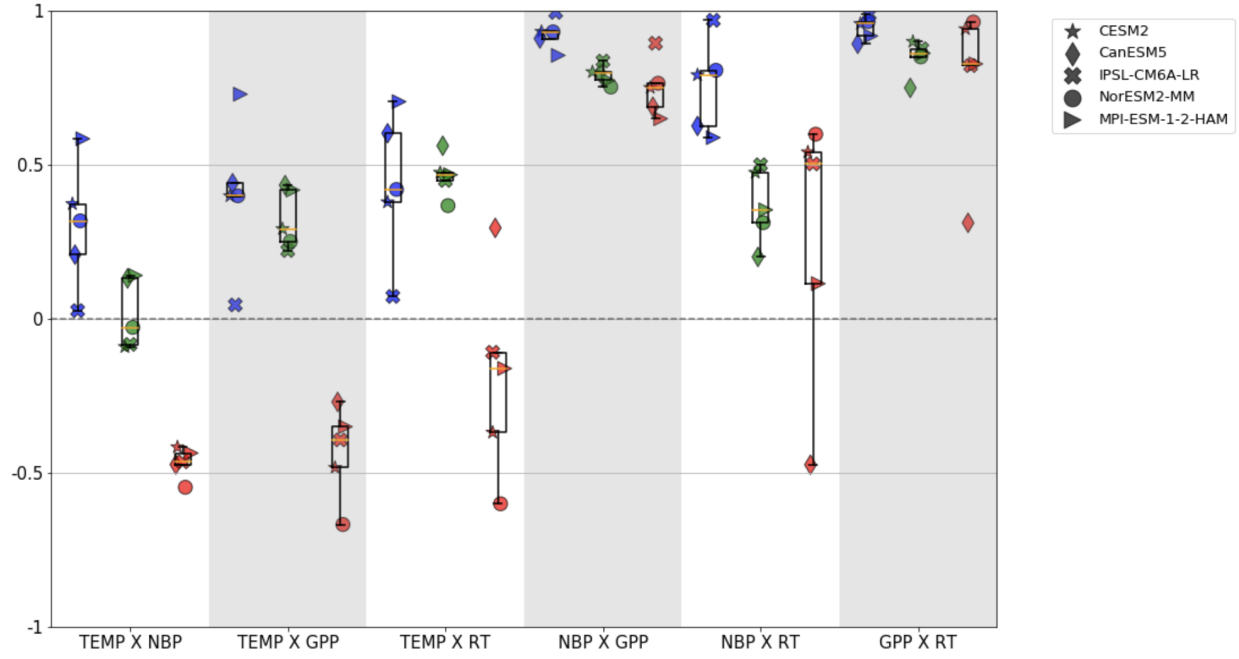

Figure 4. Scatter plots of correlations of detrended and deseasonalized zonaly aggregate growing season data for 5 ESMs. The blue shapes use data from the polar region, the green shapes use data from the temperate region, and the red shapes use data from the tropical region.

Discussion

The use of simulation data imparts uncertainty on our results. As discussed in the results section, each model has its own bias that influences our correlation values. We chose to use a model that showed results in the middle of the range to prevent over correlation of our variables. Our results also do not differentiate between correlations of the actual carbon fluxes and correlation between the mechanisms controlling the fluxes. Either way, understanding that relationship will improve our knowledge of the carbon cycle and our ability to make carbon projections.

The models showed the greatest agreement in correlation strength and sign in the temperate region. The northern hemisphere temperate ecosystem is where we have the most observational data. The strong seasonal pattern of the temperate region provides a good framework to shape the model around, combined with ample verification data to make the models the most accurate in this region. The model spreads are

largest in the tropical region (especially for RT correlations). Using similar logic, the year-round growing season and lack of observational data in this region limit the accuracy and agreement of ESM's carbon cycle data.

Based on the relationships we have quantified, we can expect that a future warming scenario of 2 ºC would cause NBP in the polar region to increase by 0.74 Pg C year^{-1}, GPP to increase by 1.86 Pg C year^{-1}, RT to increase by 0.92 Pg C year^{-1} due to temperature increases and 1.36 Pg C year^{-1} due to GPP increases. The correlation of GPP and RT increases the net land sink of the polar region in a future warming scenario. For the temperate region, we can expect NBP to decrease by 0.30 Pg C year^{-1}, GPP to increase by 1.92 Pg C year^{-1}, RT to increase by 2.16 Pg C year^{-1} due to temperature increases, and 1.07 Pg C year^{-1} due to GPP increases. The GPP and RT relationship for the temperate region will increase the net land source in a warming scenario because of the additional increase in respiration due to GPP. And for the tropical region, we can expect NBP to decrease by 1.32 Pg C year^{-1}, GPP to decrease by 3.24 Pg C year^{-1}, RT to decrease by 1.88 Pg C year^{-1} due to temperature increases, and 2.33 Pg C year -1 due to GPP decreases. Under this future warming scenario, the positive correlation of GPP with RT decreases the net land source of the tropics by reducing respiration with reduced GPP.

The models suggest that high latitude terrestrial ecosystems are becoming more of a carbon sink. The opposite is true for the lower latitudes. Our results show that warming temperatures increase respiration faster than production, enhancing the carbon source of the tropical biosphere. Since the polar regions are warming faster than the tropics due to arctic amplification (Cohen et al., 2014), we speculate that in the short term the net land sink of the poles will increase more than the net source of the tropics, even though our numbers (polar NBP increase of 0.74 Pg C year^{-1} and tropical NBP of 1.32 Pg C year^{-1}) would indicate otherwise.

Being able to quantify the relationship between these variables will allow us to improve our modeling of the carbon cycle. Observational data sets play a key role in this as they provide a metric to compare model outputs to and provide accurate boundary/initial conditions from which to force the model. Carbon cycle fluxes can not be directly measured at large spatial scales which requires the use of models or upscaling methodologies. Our understanding of the dynamics at play for the IAV of the carbon cycle is limited, so quantifying how NBP, GPP, and HR are affected by each other and temperature will improve how we parameterize the carbon cycle in ESMs and strengthen the quality of our future climate projections.

Conclusion

We have quantified the relationships between the IAV of carbon fluxes and temperature. Using carbon flux and temperature data from 1995 to 2015 from five CMIP6 models, we found that increasing temperatures tend to increase GPP in the mid to high latitudes and reduce GPP in the low latitudes. When coupled with the increase in respiration with temperature, higher temperatures reduce carbon storage everywhere except the high latitudes. Considering these patterns in a warming world, we can expect a reduction in the mid to low latitude land carbon sink and a strengthening of the high latitude sink.

Work Cited

Bruhwiler, L., A. M. Michalak, R. Birdsey, J. B. Fisher, R. A. Houghton, D. N. Huntzinger, and J. B. Miller, 2018: Chapter 1: Overview of the global carbon cycle. In Second State of the Carbon Cycle Report (SOCCR2): A Sustained Assessment Report [Cavallaro, N., G. Shrestha, R. Birdsey, M. A. Mayes, R. G. Najjar, S. C. Reed, P. Romero-Lankao, and Z. Zhu (eds.)]. U.S. Global Change Research Program, Washington, DC, USA, pp. 42-70, https://doi.org/10.7930/SOCCR2.2018.Ch1.

Chapin F.S., Matson P.A., Vitousek P.M. (2011) Decomposition and Ecosystem Carbon Budgets. In: Principles of Terrestrial Ecosystem Ecology. Springer, New York, NY. https://doi.org/10.1007/978-1-4419-9504-9_7

Cohen, J., Screen, J., Furtado, J. *et al.* Recent Arctic amplification and extreme mid-latitude weather. *Nature Geosci* 7, 627–637 (2014). https://doi.org/10.1038/ngeo2234

Dahlman, Rebecca Lindsey and LuAnn. "Climate Change: Global Temperature." *Climate Change: Global Temperature | NOAA Climate.gov*, National Oceanic and Atmospheric Administration, 15 Mar. 2021, https://www.climate.gov/news-features/understanding-climate/climate-change-global-temperature .

Danabasoglu, G., Lamarque, J.-F., Bacmeister, J., Bailey, D. A., DuVivier, A. K., Edwards, J., et al. (2020). The Community Earth System Model Version 2 (CESM2). *Journal of Advances in Modeling Earth Systems*, 12, e2019MS001916. https://doi.org/10.1029/2019MS001916

Eyring, V., Bony, S., Meehl, G. A., Senior, C. A., Stevens, B., Stouffer, R. J., and Taylor, K. E.: Overview of the Coupled Model Intercomparison Project Phase 6 (CMIP6) experimental design and organization, Geosci. Model Dev., 9, 1937–1958, https://doi.org/10.5194/gmd-9-1937-2016, 2016.

Lindsey, Rebecca. "Climate Change: Atmospheric Carbon Dioxide." *Climate Change: Atmospheric Carbon Dioxide | NOAA Climate.gov*, National Oceanic and Atmospheric Administration, 14 Aug. 2020, https://www.climate.gov/news-features/understanding-climate/climate-change-atmospheric-carbon-dioxide.

"Ocean-Atmosphere CO2 Exchange." *Science On a Sphere*, National Oceanic and Atmospheric Administration, 12 Nov. 2015, https://sos.noaa.gov/catalog/datasets/ocean-atmosphere-co2-exchange/.

Ritchie, Hannah, and Max Roser. "CO2 Emissions." *Our World in Data*, Our Wold in Data, 11 May 2020, https://ourworldindata.org/co2-emissions.

Wang, W., et al. “Variations in Atmospheric CO2 Growth Rates Coupled with Tropical Temperature.” *Proceedings of the National Academy of Sciences*, vol. 110, no. 32, 2013, pp. 13061–13066., https://doi.org/10.1073/pnas.1219683110.